Venkatraman, R. K., Kayal, S., Barak, A., Orr-Ewing, A. J., & Umapathy, S. (2018). Intermolecular Hydrogen Bonding Controlled Intersystem Crossing Rates of Benzophenone. *Journal of Physical Chemistry Letters*, *9*(7), 1642-1648. https://doi.org/10.1021/acs.jpclett.8b00345

Intermolecular Hydrogen Bonding Controlled Intersystem Crossing Rates of Benzophenone

Ravi Kumar Venkatraman[†‡], Surajit Kayal[‡], Arvind Barak[‡], Andrew J. Orr-Ewing[†] and Siva Umapathy[#‡*].*

‡Department of Inorganic and Physical Chemistry, Indian Institute of Science, Bangalore 560012, India

#Department of Instrumentation and Applied Physics, Indian Institute of Science, Bangalore 560012, India

†School of Chemistry, University of Bristol, Cantock's Close, Bristol BS8 1TS, UK.

AUTHOR INFORMATION

Corresponding Authors

* Siva Umapathy. Email: umapathy@ipc.iisc.ernet.in.

* Andrew J Orr-Ewing. Email: a.orr-ewing@bristol.ac.uk

ABSTRACT: Solvation plays a critical role in various physicochemical and biological processes. Here, the rate of intersystem crossing (ISC) of benzophenone from its $S_1(n\pi^*)$ state to its triplet manifold of states is shown to be modified by hydrogen-bonding interactions with protic solvent molecules. We selectively photo-excite benzophenone with its carbonyl group either solvent coordinated or uncoordinated by tuning the excitation wavelength to the band center (λ = 340 nm) or the long-wavelength edge (λ = 380 nm) of its $\pi^* \leftarrow n$ absorption band. A combination of ultrafast absorption and Raman spectroscopy shows that the hydrogen bonding interaction increases the time constant for ISC from < 200 fs to 1.7 ± 0.2 ps for benzophenone in CH_3OH. The spectroscopic evidence suggests that the preferred pathway for ISC is from the $S_1(n\pi^*)$ to the $T_2(\pi\pi^*)$ state, with the rate of internal conversion from $T_2(\pi\pi^*)$ to $T_1(n\pi^*)$ controlled by solvent quenching of excess vibrational energy.

TOC GRAPHIC

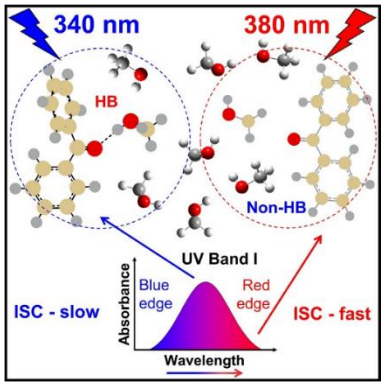

KEYWORDS Transient absorption spectroscopy; Ultrafast Raman loss spectroscopy; Solvent effects; Kinetic isotope effect; Red-edge excitation effect; Hydrogen bonding.

Benzophenone (Bzp) serves as an archetypal molecular system for understanding the fundamental photochemistry of aromatic ketones.[1-4] Both Bzp and its derivatives have been studied extensively owing to their technologically relevant applications,[5] which include use as sunscreens,[6] DNA photosensitizers,[7-9] and photocatalysts.[10] Ultraviolet (UV) excited benzophenone is known to undergo ultrafast conversion from singlet to triplet states, a property which is exploited in some of the above applications, but the intersystem crossing (ISC) mechanism remains the subject of experimental and computational investigations.[11-21] Here, we examine how the ISC is modified by hydrogen bonding in a protic solvent.

The two lowest singlet and triplet excited states of Bzp have nπ* and ππ* character. A nanosecond time-resolved infrared spectroscopy study indicated that the minima in the potential energy surfaces of the $T_2(\pi\pi^*)$ and $S_1(n\pi^*)$ states are almost isoenergetic.[22] Therefore, after the longest wavelength photo-excitation, hereafter referred to as band I and described as a $\pi^* \leftarrow n$ transition localized in the carbonyl group, two plausible pathways from the resulting $S_1(n\pi^*)$ state can populate the lowest triplet excited state, $T_1(n\pi^*)$: i) direct ISC from $S_1(n\pi^*)$ to $T_1(n\pi^*)$; or ii) an indirect process, involving ISC from $S_1(n\pi^*)$ to $T_2(\pi\pi^*)$ with subsequent internal conversion (IC) to $T_1(n\pi^*)$. The latter pathway is more efficient, according to El-Sayed's rule, because it entails a change in the orbital character during the spin-orbit coupling mediated ISC process.[23] Two recent *ab initio* molecular dynamics studies obtained contradictory results for the ISC mechanism, one favouring the indirect and other the direct pathway, highlighting the intricacies of a correct theoretical treatment.[18-19] Furthermore, these simulations were carried out for isolated molecules in the gas-phase, and are therefore removed from the technological applications of Bzp photochemistry which all involve a solvent environment.

Solvent plays an active instead of a mere spectator role in various physicochemical and biological processes,[24-30] with the diverse solute-solvent interactions broadly classified as non-specific or specific.[31-34] A recent study of the solvatochromic behaviour of Bzp identified a linear correlation between the shifts in carbonyl stretching band vibrational frequencies observed by Raman spectroscopy and the UV band I ($\pi^*\leftarrow n$) electronic transition frequencies with changing solvent polarity.[33] In protic solvents, there are two distinct solvation states, with either a hydrogen bonded (HB) or a dangling carbonyl group of Bzp, and the observed correlation is consistent with selective excitation of Bzp molecules with a dangling carbonyl at the long-wavelength side of band I.[33] In contrast, the shorter wavelength regions of band I correspond predominantly to absorption by Bzp molecules with hydrogen-bonded carbonyl groups, with a minor contribution from excitation to higher vibronic levels of the S_1 state of Bzp with a dangling carbonyl. This interpretation has been confirmed by resonance Raman spectroscopy studies of Bzp solutions in methanol, as reported below. The longer wavelength photo-selective excitation of a distinct solvation state of Bzp is an example of a red-edge excitation effect (REEE). REEE has been explored widely using fluorescence spectroscopy methods,[35-36] but we exploit it here on the $S_1 \leftarrow S_0$ band for Bzp in methanol to examine the photo-induced excited state dynamics using several complementary spectroscopic techniques.

The main objectives of the current study of Bzp in solution are: i) to elucidate the relative importance of the direct and indirect pathways populating the T_1 state of Bzp; and ii) to understand solvation-state selective excitation across band I and its implications for the subsequent photochemistry. To address these objectives, we have carried out a comprehensive analysis of the ultrafast dynamics of Bzp in methanol (chosen as a representative protic solvent)

using steady-state resonance Raman, femtosecond time-resolved electronic and vibrational absorption, and ultrafast Raman loss (URL) spectroscopic experiments.

Detailed descriptions of the various experimental methods adopted in this work are published elsewhere,[32, 37-41] and the supporting information provides a brief summary of these and the computational methods used. To verify that REEE applies to Bzp in methanol, we carried out resonance Raman spectroscopy experiments because they show selective enhancement of the vibrational modes coupled to the chromophore on resonant electronic excitation.[32, 42-43] Figure S1 of the supporting information shows Resonance Raman spectra of Bzp in methanol at several different excitation wavelengths across the $\pi^*\leftarrow n$ carbonyl band. The spectra reveal two carbonyl peaks corresponding to distinct solvation states, namely the dangling carbonyl (for excitation to longer wavelengths in band I) and the hydrogen-bonded carbonyl (to shorter excitation wavelengths). Figure 1 depicts the band I absorption spectrum (on the right ordinate) and the relative Raman intensities of HB and dangling carbonyl peaks (on the left ordinate) as a function of UV excitation wavelength. The relative intensities were obtained by taking the ratio of the integrated areas of the corresponding two peaks in the resonance Raman spectra, as shown in Figure S1. The intensity ratios were fitted to a sigmoidal function with an inflection point at λ_i = (367 ± 1) nm. The intensity ratio at 398 nm accounts for pre-resonant Raman contributions to the measurements and therefore serves as a baseline offset for estimating relative populations of HB to dangling carbonyl motifs for Bzp. Excitation at longer wavelengths than 367 nm preferentially excites Bzp molecules with a dangling carbonyl, whereas wavelengths below 367 nm (i.e. those in proximity to the peak wavelength, λ_{max}, of the band) favour Bzp with a hydrogen-bonded (to methanol) carbonyl. These observations can be accounted for by a

hydrogen-bond weakening mechanism for the S_1 state of Bzp in methanol, with the vibronic origin of the $S_1 \leftarrow S_0$ band shifted to higher energy than for Bzp with a dangling carbonyl.

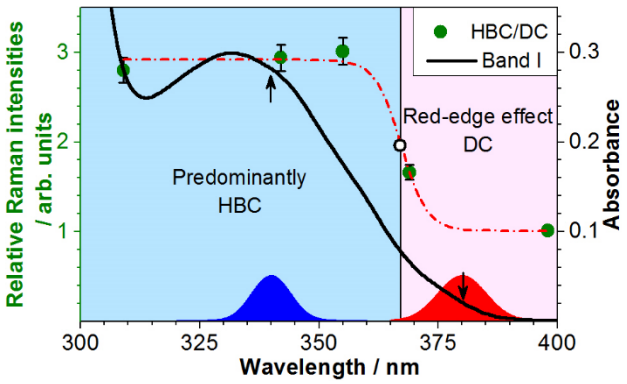

Figure 1. The effect of hydrogen bonding on the electronic absorption spectrum of benzophenone in methanol. Right ordinate and solid black line: UV-Vis absorption spectrum of Bzp in CH_3OH. Left ordinate and solid green circles: Resonance Raman intensity ratios for hydrogen bonded carbonyl (HBC) and dangling carbonyl (DC) groups in dissolved Bzp. A sigmoidal fit to the ratio of resonance Raman intensities (dash-dotted red line) shows an inflection point at 367 nm (open white circle). The arrows depict the 340 and 380-nm excitation wavelengths chosen in the ultrafast spectroscopy experiments. The red and blue Gaussian functions at the bottom represent the FT limited spectral bandwidths (nm) of the 340 and 380 nm excitation pulses, respectively.

We first describe time-resolved electronic absorption spectroscopy (TEAS) of Bzp in methanol, using excitation wavelengths of 380 and 340 nm, as indicated in Figure 1. The Fourier transform (FT) limited bandwidths of these excitation pulses are represented by Gaussian functions in the figure. The chosen centre wavelengths will specifically excite sub-ensembles of HB and non-HB (i.e. dangling carbonyl) Bzp in methanol. Representative TEA spectra of Bzp in methanol obtained at the two excitation wavelengths are shown in Figure 2, and are characterised by two dominant features: i) a band at ~570 nm with a shoulder at ~535 nm at early times (hereafter called band A); and ii) a relatively broad band at ~530 nm, with a shoulder at ~610 nm, which

develops at later times (band B). The latter feature persists up to ~ 1.4 ns, corresponding to the maximum time delay that can be achieved with our ultrafast laser setup.

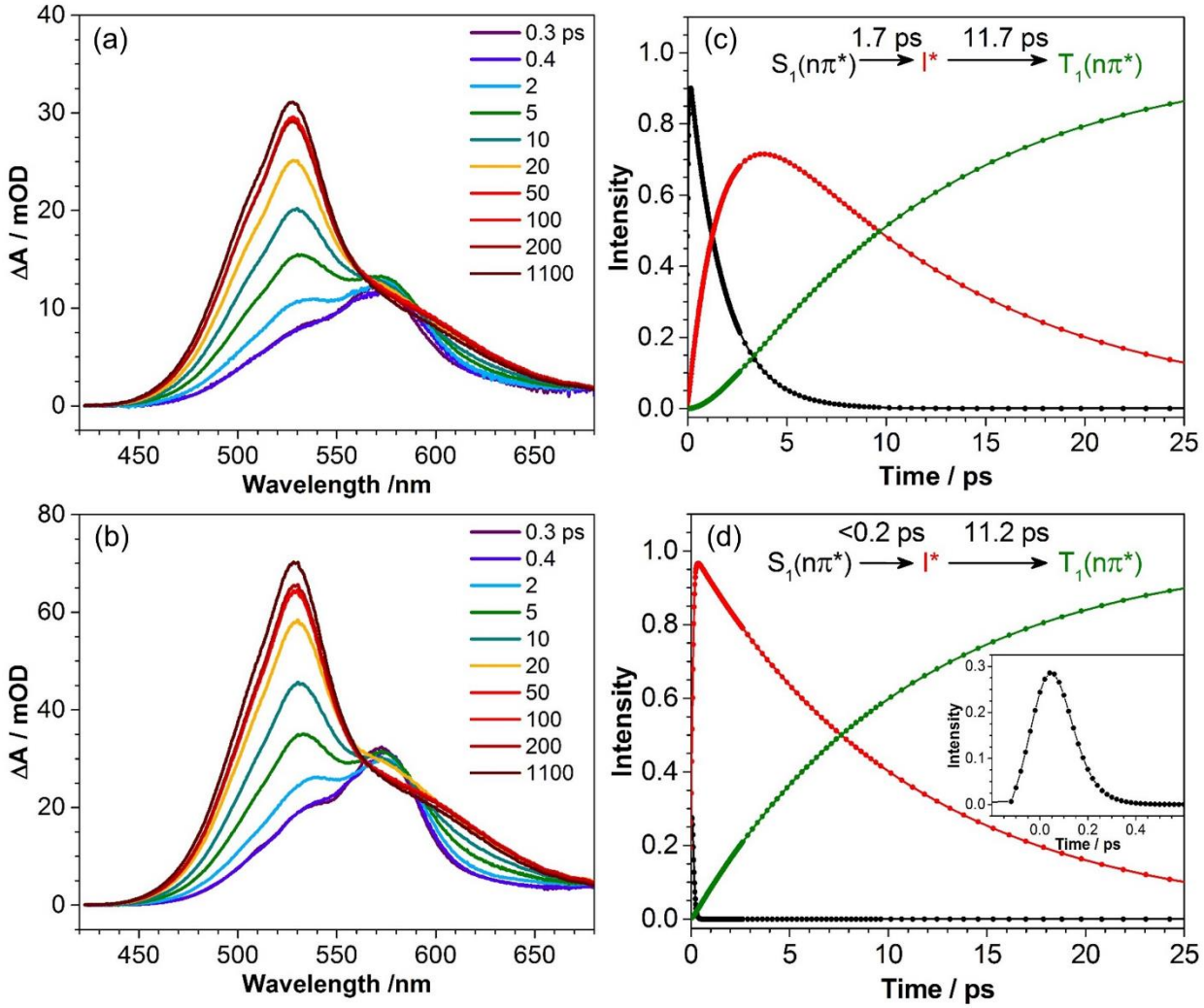

Figure 2. Time-resolved electronic absorption spectra of Bzp in CH_3OH at two different excitation wavelengths (a) 340 and (b) 380 nm. The corresponding kinetics of three different components obtained from the decay associated spectra of Bzp are shown at excitation wavelengths of (c) 340 nm and (d) 380 nm. (See Figure S2 for decay associated spectra of Bzp in CH_3OH).

To investigate the different contributions to the TEA spectra, a global fitting analysis was carried out with a sequential kinetic scheme. Three different components were obtained for both

excitation wavelengths, as shown in Figure S2. The components are assigned as: i) the S_1 state prepared directly by absorption at the UV laser wavelength; ii) an intermediate excited state species denoted I*; and iii) the long-lived T_1 state. The assignments of features to the S_1 and T_1 states are based on band positions and kinetic behaviour reported in previous publications, [2, 11-14, 22] and will be discussed further below.

For 340 nm excitation [see Figure 2(c)], the S_1 state population decays exponentially to the intermediate with a lifetime of 1.70 ± 0.15 ps, and this intermediate species subsequently decays to the T_1 state with a time constant of 11.7 ± 0.3 ps. In contrast, for 380 nm excitation [see Figure 2(d)], the intermediate grows within the instrument response function *i.e.* < 0.2 ps [see inset in Figure (2d)] and decays to the T_1 state with a time constant of 11.2 ± 0.2 ps. To confirm that the observed kinetic differences are not due to excess energy deposited in the Franck-Condon modes by the shorter-wavelength pump pulse, we also carried out TEA spectroscopy of Bzp in aprotic dipolar (acetonitrile) and non-dipolar (n-hexane) solvents at different excitation wavelengths. In all cases, the observed kinetics were similar to those for the 380 nm excitation in MeOH (see Table S1), and were found to be independent of excitation wavelength. Since absorption at longer and shorter wavelengths in band I of Bzp in MeOH corresponds to preferential excitation of the dangling and the HB carbonyl structures, respectively, we attribute the slower early time time-response for 340 nm excitation to HB interactions. To explore this hypothesis further, we compared TEA spectra for Bzp in CH_3OH and CD_3OD solvents following excitation at 340 nm.

The time constants obtained with different solvent isotopologues at 340 and 380 nm excitation wavelengths are reported in Table 1. The change of solvent from CH_3OH to CD_3OD has greater influence on the faster component of the sequential kinetics, with no significant effect on the slower component (see also Figure S3). In the classical limit ($h\nu_{HB} < k_BT$), the kinetic isotopic

effect $\frac{k_H}{k_D}$ is approximately the inverse ratio of the square roots of the effective masses of the atoms involved in the reaction coordinate,[44] in this case the H/D-atom of the HB. The observed kinetic isotope effect was obtained to be 1.48 ± 0.22, in accord with this estimation. The rise times of band B in CH_3OH and CD_3OD solvents are independent of solvent isotopologue within the uncertainties. The HB motion therefore appears to be a critical reaction coordinate bottleneck for the first step in the relaxation of the S_1 state of Bzp.

Table 1. Time Constants from TEAS Measurements for Bzp in Methanol and Methanol-d_4 at Different Excitation Wavelengths.

Excitation wavelength (nm)	Solvent	Time constant (ps)	
		τ_1	τ_2
340	CH_3OH	1.70 ± 0.15	11.7 ± 0.3
	CD_3OD	2.52 ± 0.16	11.0 ± 0.1
380	CH_3OH	< 0.2	11.2 ± 0.2
	CD_3OD	< 0.2	11.4 ± 0.1

To investigate further the photochemical dynamics of Bzp, we performed time-resolved vibrational absorption spectroscopy (TVAS) measurements of Bzp in CD_3OD (chosen for its IR transparency at the mid-IR probe wavelengths of interest). Figure 3(a) depicts the TVA spectra of Bzp in CD_3OD for 340 nm excitation. The prominent peaks at 1470 and 1158 cm^{-1} (marked by asterisks) are assigned in part to the ring C-H rocking mode and ring C-H scissoring modes in the S_1 state, on the basis of time-dependent density functional theory (TD-DFT) calculations at the B3LYP/cc-pVTZ level of theory (see the Supporting Information). Further peaks at 1555 and

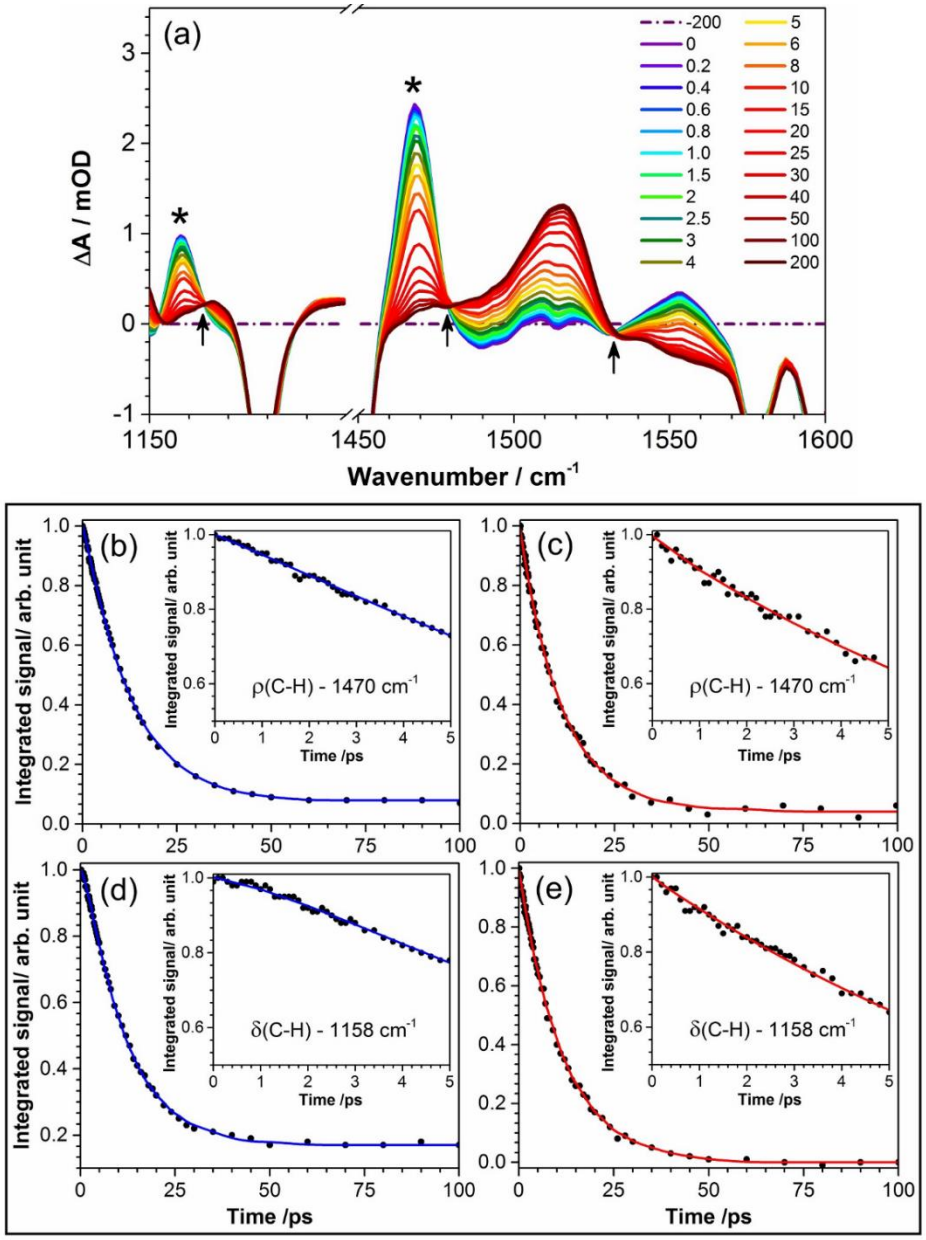

Figure 3. (a) Time-resolved vibrational absorption spectra of Bzp in CD_3OD after 340-nm excitation. The arrows indicate isosbestic points, and the inset color key identifies the time delays (in ps) at which each spectrum was obtained. The time-dependent integrated band intensities of the prominent peaks centered at 1470 and 1158 cm^{-1}, and indicated by asterisks in (a), are shown at excitation wavelengths of 340 nm in panels (b) and (d), and 380 nm in panels (c) and (e). The insets show expanded views at early time delays. Solid lines are bi-exponential fits.

1158 cm^{-1} are also assigned to the S_1 state.

The arrows in Figure 3(a) indicate isosbestic points observed between different vibrational features, suggesting transformation from one species to another. The peak at 1517 cm^{-1} is assigned to the T_1 state because of its long lifetimes (> 1.4 ns), as shown in Fig S5. This assignment is supported by a previous nanosecond time-resolved IR spectroscopic study of Bzp,[22] and is further corroborated by TD-DFT calculations. These calculations also suggest that the weak peaks at 1474 and 1167 cm^{-1} observed at longer times delays derive from the T_1 state. Table S2 provides a summary of various vibrational peaks observed from TVAS experiments and their assignments based on TD-DFT calculations.

Comparison of the early time curvatures of the time-dependent integrated band intensities in the insets to Figures 3(b) and (c) suggests subtly different kinetics of the 1470 cm^{-1} peak at the two excitation wavelengths of 340 and 380 nm. These differences are also apparent in the corresponding time-dependent data for the 1158 cm^{-1} peak, as seen in the insets to Figures 3(d) and (e). The evolving band intensities were fitted to bi-exponential functions (see equation S1 of the Supporting Information), and the amplitudes and time constants obtained from the fitting are reported in Table S3. At 340 nm, the fits for the 1470 cm^{-1} peak data revealed an early rise (with time constant 2.51 ± 0.13 ps) and a later decay (12.1 ± 0.3 ps) which match the corresponding time constants obtained by TEAS for Bzp in CD_3OD. At 380 nm, an initial instrument response function limited rise (< 0.2 ps) and decay kinetics with time constant 11.0 ± 0.3 ps were obtained, again in accord with TEAS measurements. The time dependences of the 1158 cm^{-1} feature at the two excitation wavelengths agree with those of the 1470 cm^{-1} band, as is shown in Figures 3 (d) and (e) and Table S3. The kinetics of other vibrational features are displayed in Figure S5. The negative signals in the transient spectra match the positions of absorption bands

in the steady-state state FTIR spectrum of Bzp in CD_3OD and are therefore assigned to the ground state bleach. They show no recovery within 1.4 ns because of the high quantum yield and long lifetime of the T_1 state.

Two possible mechanisms could plausibly account for the early time rises in the bands centered at 1470 and 1158 cm^{-1}, and the corresponding kinetics observed by TEAS following 340 nm excitation. The first possibility is vibrational cooling in the S_1 state, followed by ISC to the T_1 state (a direct mechanism), and the second is motion of an initially formed wave packet from the Franck-Condon region to an intermediate state (denoted I* in Fig 2, argued later to be the T_2 state), followed by relaxation to the T_1 state (an indirect mechanism). The first hypothesis is questionable because the kinetics of Bzp ISC in aprotic solvents are independent of excitation wavelength, and hence vibrational cooling of S_1 (see Table S1). The second interpretation is supported by the decomposition of the TEA spectra, but requires vibrational absorption bands of the I* intermediate to contribute to the TVA spectra at 1470 and 1158 cm^{-1} (a reasonable argument for strongly mixed S_1 and I* states). On the basis of recently reported calculations for Bzp photochemical dynamics,[19] and arguments presented below, the most likely assignment of the intermediate is to the $T_2(\pi\pi^*)$ state.

The $S_1/T_1(n\pi^*)$, and the $T_2(\pi\pi^*)$ states of Bzp[33] and similar aromatic ketones[31-32, 42, 45] undergo HB weakening and strengthening, respectively, compared to the ground state (S_0). Hydrogen bonding destabilizes the S_1 state, and photo-excitation of Bzp with an HB carbonyl to the S_1 state will induce reorganization along the HB carbonyl solvation coordinate. The different HB responses of the S_1 and T_2 state energies initially push these states apart, but affect the S_1 and T_1 state energies in a similar fashion. Thus, the observed solvent kinetic isotope effect supports the

proposition that I* has $T_2(\pi\pi^*)$ character because HB reorganization is required to bring the $S_1(n\pi^*)$ and the $T_2(\pi\pi^*)$ states closer to degeneracy to facilitate the ISC.

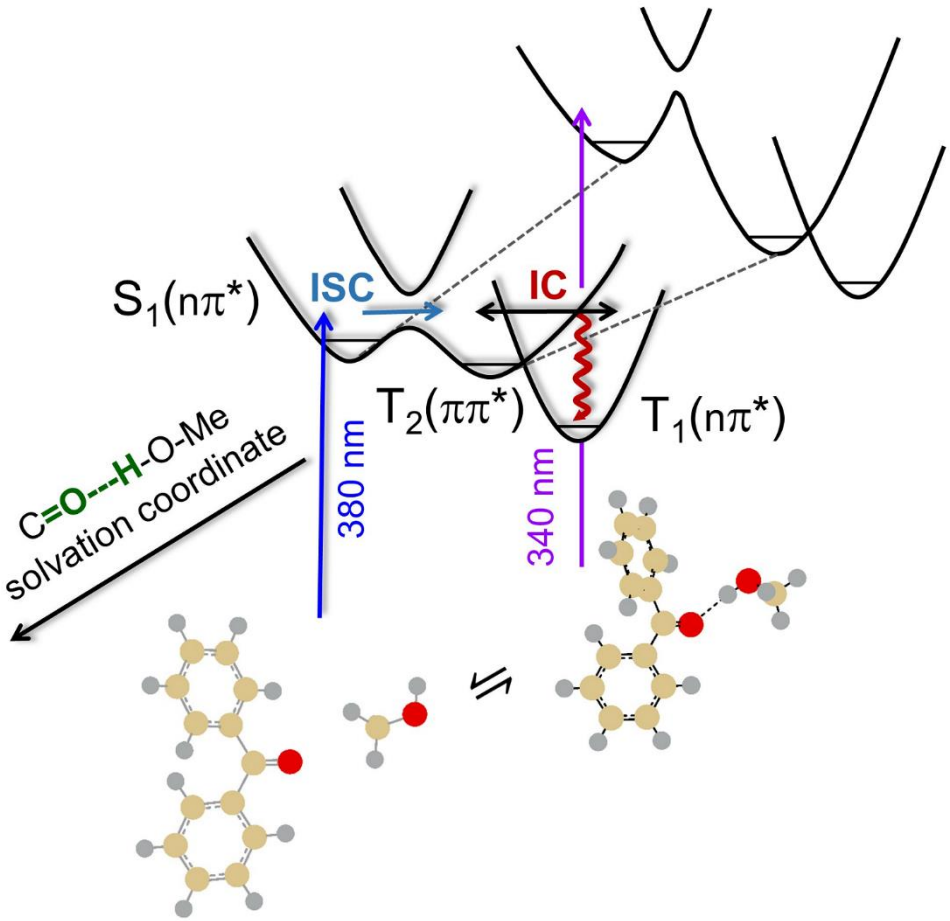

Figure 4. Schematic representation of photo-selective excitation of distinct solvation states, corresponding to Bzp with dangling and HB carbonyl groups at 380 and 340 nm respectively, and their associated dynamics. See the main text for further details.

This picture of dynamic solvation effects requires a two-dimensional reaction coordinate for the ISC mechanism of Bzp: one coordinate lies along the intramolecular ISC pathway from S_1 to the triplet manifold, and the second involves the solvent coordinate, as shown schematically in Figure 4. After 380-nm photo-excitation of Bzp with a dangling carbonyl to the $S_1(n\pi^*)$ state, the

initial wave packet evolves rapidly from the Franck-Condon region to a crossing with the T_2 state along an almost barrierless pathway, with ISC induced by spin-orbit coupling.[44] In contrast, intermolecular HB reorganization acts as a bottleneck for the excited state dynamics of Bzp with an HB carbonyl selected by 340-nm excitation, as underpinned by our measured solvent kinetic isotope effects.

Accordingly, we can explain our observations in terms of the indirect pathway for T_1 population, invoking the $T_2(\pi\pi^*)$ state as an intermediate before relaxation to the T_1 state. This interpretation does not rule out the possibility for a direct $S_1 \rightarrow T_1$ contribution, but the indirect mechanism is further substantiated by a recent *ab initio* molecular dynamics simulation of Bzp in the gas phase.[19]

Table 2. Time Constants from URLS Measurements for Changes to the 992 cm^{-1} Band of the T_1 State of Bzp in Methanol after 340-nm Excitation.

	Time constant (ps)
	τ_1
Peak intensity	12.6 ± 1.0
Peak position	14.9 ± 2.1

The slower component of the kinetics, observed for both excitation wavelengths, is assigned to internal conversion between the triplet states. It is at first sight surprising that the $T_2 \rightarrow T_1$ IC, which occurs with a time constant of ~ 11 ps, is slower by an order of magnitude than the ISC rate. However, similar timescales have been reported for IC between the triplet states of various aromatic ketones,[45-47] and attributed either to thermal[45-46] or kinetic[19] equilibrium. For Bzp in solution, we propose that the IC rate will be dictated by the vibrational energy transfer rate to the solvent, which quenches the rapid exchange between the T_2 and T_1 states by relaxation to the

minimum on the T_1 state. We therefore performed additional ultrafast Raman loss spectroscopy (URLS) measurements to determine the VET timescale. The URL spectra and kinetics profiles obtained from band intensities and center positions for the ring breathing vibrational mode in the T_1 state of Bzp (at 992 cm^{-1}) are shown in Figures S6 and S7. The various time constants obtained from the URL spectra are summarized in Table 2. The observed shift of the peak of the 992 cm^{-1} band is characteristic of VET to a solvent,[48] and the kinetics indicate that the $T_2 \rightarrow T_1$ IC is indeed controlled by loss of the excess vibrational energy in the T_1 state to the solvent environment. The supporting information provides a more detailed discussion.

In summary, we report observation of photo-selective excitation of sub-ensembles of different solvation states of Bzp in methanol, corresponding to either dangling or hydrogen bonded carbonyl groups, by exciting to longer or shorter wavelength in the Bzp $\pi^* \leftarrow n$ electronic excitation band. This photo-selectivity is corroborated by resonance Raman spectroscopy. The $S_1(n\pi^*)$ and $T_2(\pi\pi^*)$ states exhibit HB weakening and strengthening mechanisms, respectively, and the hydrogen-bonding solvation coordinate therefore influences the $S_1 \rightarrow T_2$ ISC rate. We determine the ISC time constants for Bzp in CH_3OH with dangling and HB carbonyl groups to be < 0.2 and 1.7 ps, respectively. The build-up of the T_1 state population by IC from the T_2 state is slower, with a time constant of ~11 ps because VET from vibrationally hot T_1 levels to the solvent environment is required to quench the kinetic equilibrium between the T_2 and T_1 state populations. The VET to the solvent is revealed directly by ultrafast Raman loss spectroscopy. These findings indicate the pathway to the T_1 state passes mostly through an intermediate with $T_2(\pi\pi^*)$ character, with a rate which is influenced by the micro-solvation environment of the Bzp. The solvent-modified excited state dynamics are significant for the photochemical pathways followed in diverse applications of Bzp. Moreover, the conclusions from this study are

expected to extend to the photochemical properties of other aromatic ketone compounds, and wider classes of molecules with carbonyl functionality.

ASSOCIATED CONTENT

Supporting Information.

The following content is available free of charge. Experimental and Computational Methods. Resonance Raman spectra of Bzp in methanol at various excitation wavelengths. Decay associated spectra of Bzp in methanol at two different excitation wavelengths. Excitation wavelength dependence of time constants from TEAS measurements of Bzp in aprotic solvents. Solvent isotopic effect on the rate of Bzp dynamics. Time resolved vibrational absorption spectra of Bzp in CD_3OD. Vibrational assignments of peaks observed in TVAS experiments. Fits of TVAS peaks at 1470 and 1158 cm^{-1} to a bi-exponential model. Kinetics of various vibrational peaks observed in TVAS experiments. Kinetics of the ring breathing mode of Bzp in the T_1 state obtained from URLS experiments. Kinetics of population dynamics of the T_1 state and the vibrational energy transfer rate to the solvent obtained from URLS measurements. Further text description of ultrafast Raman loss spectroscopy investigation of vibrational energy transfer rate from the hot T_1 state of Bzp to the solvent.

All experimental data are archived in the University of Bristol's Research Data Storage Facility (DOI: https://doi.org/10.5523/bris.3n569v5dklhm020vkoudxclw2m)

AUTHOR INFORMATION

The authors declare no competing financial interests.

ACKNOWLEDGMENT

The Bristol laboratory was established with funding from ERC Advanced Grant 290966 CAPRI, and RKV acknowledges the Royal Society (London, UK) and the SERB (India) for award of a SERB-Royal Society Newton International Fellowship. We thank Philip Coulter (University of Bristol) for help with the experiments and for valuable discussions. SK and AB acknowledge the Council of Scientific and Industrial Research (CSIR) for a research fellowship. SU acknowledges the Defence Research and Development Organisation (DRDO) for financial assistance and the Department of Science and Technology (DST) for a J.C. Bose Fellowship.

REFERENCES

1. Porter, G.; Suppan, P. Primary Photochemical Processes in Aromatic Molecules. 12. Excited States of Benzophenone Derivatives. *Trans. Faraday Soc.* **1965,** *61*, 1664-1673.

2. Porter, G.; Wilkinson, F. Primary Photochemical Processes in Aromatic Molecules. 5. Flash Photolysis of Benzophenone in Solution. *Trans. Faraday Soc.* **1961,** *57*, 1686-1691.

3. Wagner, P.; Park, B. S. Photoinduced Hydrogen Atom Abstraction Reaction by Carbonyl Compounds. In *Organic Photochemistry*, Padwa, A., Ed. Marcel Dekker: New York, 1991; pp 227-366.

4. Turro, N. J.; Ramamurthy, V.; Scaiano, J. C. *Modern Molecular Photochemistry of Organic Molecules*. University Science Books: Sausalito, CA., 2010.

5. Dorman, G.; Nakannura, H.; Pulsipher, A.; Prestwich, G. D. The Life of Pi Star: Exploring the Exciting and Forbidden Worlds of the Benzophenone Photophore. *Chem. Rev.* **2016,** *116*, 15284-15398.

6. Baker, L. A.; Horbury, M. D.; Greenough, S. E.; Coulter, P. M.; Karsili, T. N. V.; Roberts, G. M.; Orr-Ewing, A. J.; Ashfold, M. N. R.; Stayros, V. G. Probing the Ultrafast Energy Dissipation Mechanism of the Sunscreen Oxybenzone after UVA Irradiation. *J. Phys. Chem. Lett.* **2015,** *6*, 1363-1368.

7. Cuquerella, M. C.; Lhiaubet-Vallet, V.; Cadet, J.; Miranda, M. A. Benzophenone Photosensitized DNA Damage. *Acc. Chem. Res.* **2012,** *45*, 1558-1570.

8. Dumont, E.; Wibowo, M.; Roca-Sanjuan, D.; Garavelli, M.; Assfeld, X.; Monari, A. Resolving the Benzophenone DNA-Photosensitization Mechanism at QM/MM Level. *J. Phys. Chem. Lett.* **2015,** *6*, 576-580.

9. Dumont, E.; Monari, A. Benzophenone and DNA: Evidence for a Double Insertion Mode and Its Spectral Signature. *J. Phys. Chem. Lett.* **2013,** *4*, 4119-4124.

10. Romero, N. A.; Nicewicz, D. A. Organic Photoredox Catalysis. *Chem. Rev.* **2016,** *116*, 10075-10166.

11. Aloise, S.; Ruckebusch, C.; Blanchet, L.; Rehault, J.; Buntinx, G.; Huvenne, J. P. The Benzophenone $S_1(n, \pi^*) \rightarrow T_1(n, \pi^*)$ States Intersystem Crossing Reinvestigated by Ultrafast Absorption Spectroscopy and Multivariate Curve Resolution. *J. Phys. Chem. A* **2008,** *112*, 224-231.

12. Anderson, R. W.; Hochstrasser, R. M.; Lutz, H.; Scott, G. W. Measurements of Intersystem Crossing Kinetics Using 3545-Å Picosecond Pulses - Nitronaphthalenes and Benzophenone. *Chem. Phys. Lett.* **1974,** *28*, 153-157.

13. Damschen, D. E.; Merritt, C. D.; Perry, D. L.; Scott, G. W.; Talley, L. D. Intersystem Crossing Kinetics of Aromatic Ketones in Condensed Phase. *J. Phys. Chem.* **1978,** *82*, 2268-2272.

14. Hochstrasser, R. M.; Lutz, H.; Scott, G. W. Dynamics of Populating Lowest Triplet-State of Benzophenone Following Singlet Excitation. *Chem. Phys. Lett.* **1974,** *24*, 162-167.

15. Rentzepis, P. M. Ultrafast Processes. *Science* **1970,** *169*, 239-247.

16. Rentzepis, P. M.; Mitschele, C. J. Picosecond Spectroscopy. *Anal. Chem.* **1970,** *42*, A20-A32.

17. Spighi, G.; Gaveau, M. A.; Mestdagh, J. M.; Poisson, L.; Soep, B. Gas Phase Dynamics of Triplet Formation in Benzophenone. *Phys. Chem. Chem. Phys.* **2014,** *16*, 9610-9618.

18. Favero, L.; Granucci, G.; Persico, M. Surface Hopping Investigation of Benzophenone Excited State Dynamics. *Phys. Chem. Chem. Phys.* **2016,** *18*, 10499-10506.

19. Marazzi, M.; Mai, S.; Roca-Sanjuan, D.; Delcey, M. G.; Lindh, R.; Gonzalez, L.; Monari, A. Benzophenone Ultrafast Triplet Population: Revisiting the Kinetic Model by Surface-Hopping Dynamics. *J. Phys. Chem. Lett.* **2016,** *7*, 622-626.

20. Sergentu, D. C.; Maurice, R.; Havenith, R. W. A.; Broer, R.; Roca-Sanjuan, D. Computational Determination of the Dominant Triplet Population Mechanism in Photoexcited Benzophenone. *Phys. Chem. Chem. Phys.* **2014,** *16*, 25393-25403.

21. Zvereva, E.; Segarra-Marti, J.; Marazzi, M.; Brazard, J.; Nenov, A.; Weingart, O.; Leonard, J.; Garavelli, M.; Rivalta, I.; Dumont, E.; Assfeld, X.; Haacke, S.; Monari, A. The Effect of Solvent Relaxation in the Ultrafast Time-Resolved Spectroscopy of Solvated Benzophenone. *Photochem. Photobiol. Sci.* **2018**. In Press. DOI: 10.1039/c7pp00439g

22. Yabumoto, S.; Sato, S.; Hamaguchi, H. Vibrational and Electronic Infrared Absorption Spectra of Benzophenone in the Lowest Excited Triplet State. *Chem. Phys. Lett.* **2005,** *416*, 100-103.

23. Elsayed, M. A. Spin-Orbit Coupling and Radiationless Processes in Nitrogen Heterocyclics. *J. Chem. Phys.* **1963,** *38*, 2834-2838.

24. Bellissent-Funel, M. C.; Hassanali, A.; Havenith, M.; Henchman, R.; Pohl, P.; Sterpone, F.; van der Spoel, D.; Xu, Y.; Garcia, A. E. Water Determines the Structure and Dynamics of Proteins. *Chem. Rev.* **2016,** *116*, 7673-7697.

25. Carpenter, B. K.; Harvey, J. N.; Orr-Ewing, A. J. The Study of Reactive Intermediates in Condensed Phases. *J. Am. Chem. Soc.* **2016,** *138*, 4695-4705.

26. Dunning, G. T.; Glowacki, D. R.; Preston, T. J.; Greaves, S. J.; Greetham, G. M.; Clark, I. P.; Towrie, M.; Harvey, J. N.; Orr-Ewing, A. J. Vibrational Relaxation and Microsolvation of DF after F-Atom Reactions in Polar Solvents. *Science* **2015,** *347*, 530-533.

27. Morgenstern, K.; Marx, D.; Havenith, M.; Muhler, M. Editorial of the PCCP Themed Issue on " Solvation Science". *Phys. Chem. Chem. Phys.* **2015,** *17*, 8295-8296.

28. Orr-Ewing, A. J. Dynamics of Bimolecular Reactions in Solution. *Annu. Rev. Phys. Chem.* **2015,** *66*, 119-141.

29. Orr-Ewing, A. J. Taking the Plunge: Chemical Reaction Dynamics in Liquids. *Chem. Soc. Rev.* **2017,** *46*, 7597-7614.

30. Orr-Ewing, A. J. Perspective: Bimolecular Chemical Reaction Dynamics in Liquids. *J. Chem. Phys.* **2014,** *140*, 090901.

31. Kumar, V. R.; Ariese, F.; Umapathy, S. Triplet Excited Electronic State Switching Induced by Hydrogen Bonding: A Transient Absorption Spectroscopy and Time-Dependent DFT Study. *J. Chem. Phys.* **2016,** *144*, 114301.

32. Kumar, V. R.; Rajkumar, N.; Umapathy, S. Solvatochromism of 9,10-Phenanthrenequinone: An Electronic and Resonance Raman Spectroscopic Study. *J. Chem. Phys.* **2015,** *142*, 024305.

33. Kumar, V. R.; Verma, C.; Umapathy, S. Molecular Dynamics and Simulations Study on the Vibrational and Electronic Solvatochromism of Benzophenone. *J. Chem. Phys.* **2016,** *144*, 064302.

34. Balakrishnan, G.; Sahoo, S. K.; Chowdhury, B. K.; Umapathy, S. Understanding Solvent Effects on Structure and Reactivity of Organic Intermediates: a Raman Study. *Faraday Discuss.* **2010,** *145*, 443-466.

35. Demchenko, A. P. The Red-Edge Effects: 30 Years of Exploration. *Luminescence* **2002,** *17*, 19-42.

36. Letrun, R.; Vauthey, E. Excitation Wavelength Dependence of the Dynamics of Bimolecular Photoinduced Electron Transfer Reactions. *J. Phys. Chem. Lett.* **2014,** *5*, 1685-1690.

37. Roy, K.; Kayal, S.; Ariese, F.; Beeby, A.; Umapathy, S. Mode Specific Excited State Dynamics Study of Bis(phenylethynyl) Benzene from Ultrafast Raman Loss Spectroscopy. *J. Chem. Phys.* **2017,** *146*, 064303.

38. Grubb, M. P.; Orr-Ewing, A. J.; Ashfold, M. N. KOALA: a Program for the Processing and Decomposition of Transient Spectra. *Rev. Sci. Instrum.* **2014,** *85*, 064104.

39. Roberts, G. M.; Marroux, H. J.; Grubb, M. P.; Ashfold, M. N.; Orr-Ewing, A. J. On the Participation of Photoinduced N-H Bond Fission in Aqueous Adenine at 266 and 220 nm: a Combined Ultrafast Transient Electronic and Vibrational Absorption Spectroscopy Study. *J. Phys. Chem. A* **2014,** *118*, 11211-11225.

40. Roy, K.; Kayal, S.; Kumar, V. R.; Beeby, A.; Ariese, F.; Umapathy, S. Understanding Ultrafast Dynamics of Conformation Specific Photo-Excitation: A Femtosecond Transient Absorption and Ultrafast Raman Loss Study. *J. Phys. Chem. A* **2017,** *121*, 6538-6546.

41. Ariese, F.; Roy, K.; Ravi Kumar, V.; Sudeeksha, H. C.; Kayal, S.; Umapathy, S. Time-Resolved Spectroscopy: Instrumentation and Applications. In *Encyclopedia of Analytical Chemistry*, John Wiley & Sons, Ltd: 2006.

42. Kumar, V. R.; Umapathy, S. Solvent Effects on the Structure of the Triplet Excited State of Xanthone: a Time-Resolved Resonance Raman study. *J. Raman Spectrosc.* **2016,** *47*, 1220-1230.

43. Biswas, N.; Umapathy, S. Resonance Raman Study of the Solvent Dynamics for Ultrafast Charge Transfer Transition in 4-Nitro-4'-Dimethylamino-Azobenzene. *J. Chem. Phys.* **2003,** *118*, 5526-5536.

44. Swain, C. G.; Stivers, E. C.; Reuwer, J. F.; Schaad, L. J. Use of Hydrogen Isotope Effects to Identify the Attacking Nucleophile in the Enolization of Ketones Catalyzed by Acetic Acid. *J. Am. Chem. Soc.* **1958,** *80*, 5885-5893.

45. Kumar, V. R.; Rajkumar, N.; Ariese, F.; Umapathy, S. Direct Observation of Thermal Equilibrium of Excited Triplet States of 9,10-Phenanthrenequinone. A Time-Resolved Resonance Raman Study. *J. Phys. Chem. A* **2015,** *119*, 10147-10157.

46. Villnow, T.; Ryseck, G.; Rai-Constapel, V.; Marian, C. M.; Gilch, P. Chimeric Behavior of Excited Thioxanthone in Protic Solvents: I. Experiments. *J. Phys. Chem. A* **2014,** *118*, 11696-11707.

47. Koyama, D.; Orr-Ewing, A. J. Triplet State Formation and Quenching Dynamics of 2-Mercaptobenzothiazole in Solution. *Phys. Chem. Chem. Phys.* **2016,** *18* (37), 26224-26235.

48. Rosspeintner, A.; Lang, B.; Vauthey, E. Ultrafast Photochemistry in Liquids. *Annu. Rev. Phys. Chem.* **2013,** *64*, 247-271.